This is a repository copy of *An application of a beamforming technique, linear acoustic array and robot for pipe condition localization*.

White Rose Research Online URL for this paper:
https://eprints.whiterose.ac.uk/215683/

Version: Published Version

An application of a beamforming technique, linear acoustic array and robot for pipe condition localization

Yicheng Yu [a],[*], Pengcheng Shi [b],[c], Anton Krynkin [a], Kirill V. Horoshenkov [a]

[a] *Department of Mechanical Engineering, University of Sheffield, Mappin Street, Sheffield S1 3JD, UK*
[b] *School of Instrument and Electronics, North University of China, Taiyuan, China*
[c] *State Key Laboratory of Dynamic Measurement Technology, North University of China, Taiyuan, China*

ABSTRACT

Pipe inspection robots with sensors significantly enhance the maintenance of water systems by enabling early defect detection and reducing the risks of leaks and environmental damage. This paper introduces a sparse representation acoustic beamformer designed to locate artefacts within pipes using a short linear microphone array on a robot. The primary contributions include: (i) a new acoustic beamforming approach based on sparse representation that accurately predicts pipe conditions with a localization error within 3 % of the sensing distance; (ii) an enhanced beamforming algorithm combining plane wave and first non-axisymmetric mode, extending the frequency range from < 1300 Hz to < 2200 Hz in a 150 mm diameter pipe (an increase by 1.69 times), effectively managing unwanted acoustic reverberations and distinguishing blockages from lateral connections; and (iii) a novel robust algorithm predicting pipe length with an error margin within 2 %. This research advances acoustic sensing technologies for autonomous mobile robots inspecting buried pipes.

1. Introduction

Underground infrastructure such as buried pipes is important to urban life for transporting fluids, e.g. water, oil and gases. In the UK alone there are over 393,000 km of sewer pipes and 416,000 km of clean water mains [1]. In the EU countries the length of the drinking water pipes is more than 4.3 million km, and the wastewater pipes are longer than 3 million km [1]. There is little information on the condition of these pipes. Proactive rehabilitation of buried pipes requires reliable techniques for their condition monitoring and fault detection continuously and on a massive scale to meet the challenges due to their rapid aging, heavy usage, population growth, increasing demand for water, energy and climate change.

Autonomous robotic sensing systems [2] working in buried pipes for condition monitoring and fault detection offer the opportunity to capitalise on recent advances in acoustic and ultrasonic sensing techniques to increase the speed and coverage of pipe inspection surveys. Acoustic methods have been investigated for blockage detection and condition assessment in sewers in the past decades [3,4] due to their much further detection range, less power consumption and less computation cost compared with the Closed-Circuit Television (CCTV). Acoustically reflective artefacts including blockages and wall damage can be

localized remotely with respect to the robot position using the time delay in their acoustic echoes measured with a microphone [5]. Recently, a circular microphone array on a robotic platform was used to extend the acoustic frequency range to detect, localize and classify more reliably blockages and lateral connections in sewers using the sparse representation and support vector machine methods [6,7]. In order to determine the direction of the echo arrival, acoustic measurements were implemented sequentially at several discrete robot positions with a 0.2 m separation [6]. This approach is accurate but relatively complex requiring the robot to move in controlled steps along the pipe. It also requires the accurate knowledge of the robot's velocity. Some parts of the pipe network, e.g. manholes create a relatively reverberant environment that makes the identification of the pipe condition with acoustic waves difficult because of the multiple echoes generated in a manhole. These echoes mask the reflections from other artefacts that are further afar from the robot. Our paper proposes an array beamforming technique to determine the sound direction and to compensate for unwanted reverberation effects in a broad frequency range while the robot remains stationary. To the best of our knowledge this idea has not been tested in a pipe environment where the acoustic field is strongly multimodal.

Acoustic beamforming has been rigorously explored within the field

---

of audio processing, encompassing signal enhancement, dereverberation, and source localization [8]. Its application extends to the detection of defects in pipeline systems, such as identifying leaks in pressurized water pipes [9,10]. These applications are mainly focused on the passive sensing with beamforming algorithm for the identification of defects in pipes. Despite its widespread use, the potential of acoustic beamforming for active sensing and defect detection, such as blockage identification in sewage pipes treated as waveguides, has not been systematically explored. Active acoustic sensing by the robot can also enhance its capabilities in localization and mapping [11,7,6] as well as potential long-range acoustic communication between the robots in the pipe network [12,13,14]. This paper introduces a frequency domain beamformer designed to enable a robot to ascertain the direction of conditions within a pipe, utilizing a linear acoustic array positioned axially. This approach contrasts with time domain algorithms that apply deconvolution to estimate the impulse response for robotic localization [6]. Instead, the proposed frequency domain sparse representation method leverages phase delay across the microphone array to enhance the accuracy of directional defect localization relative to the robot in the presence of unwanted reverberation.

The structure of this paper is organised as follows. Section 2 discusses the theoretical framework of the sparse representation method to estimate the location of the artefacts in a pipe with a robot equipped with a speaker and linear microphone array. The experimental validation setup that includes a robotic sensing system and section of a typical drainage pipe is presented in Section 3. The results obtained with the beamforming technique and sparse representation method are compared in Sections 4.1 and 4.2 for plane wave regime and first non-axisymmetric mode regime, respectively. Section 4.3 discusses the proposed algorithm for the identification of the length of the pipe sections.

2. Theory

2.1. Multi-modal wave in a pipe

In the frequency domain the acoustic field in a rigid cylindrical pipe (see Fig. 1) can be expressed as the superposition of modes as suggested by Morse and Ingard [15]:

$$p(r, \theta, z, \omega) = \sum A_{mn} \varphi_{mn}(r, \theta) e^{i\gamma_{mn}z}, \tag{1}$$

where $i = \sqrt{-1}$, ω is the angular frequency, m and n are the mode indices, φ_{mn} is the mode shape function in the pipe, A_{mn} is the mode amplitude. For an empty cylindrical pipe (filled with air) with acoustically rigid and smooth walls (without considering the effects from wall
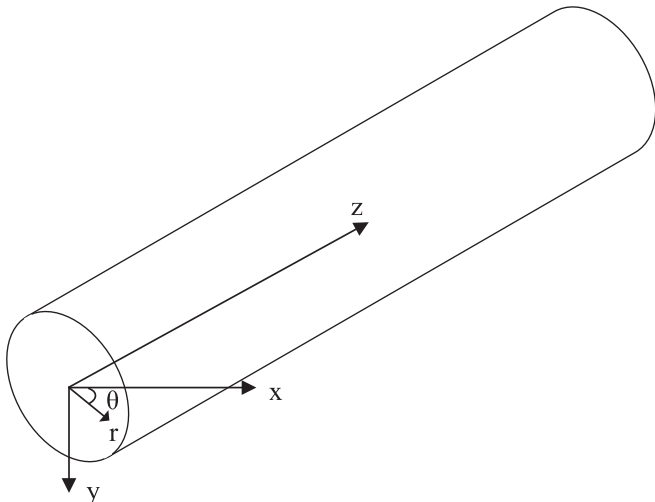

Fig. 1. The system of coordinates in a cylindrical pipe.

roughness [16]) the mode shape function is given by [15]:

$$\varphi_{mn}(r, \theta) = \cos(m\theta) J_m(k_{mn}r), \tag{2}$$

where $J_m(\bullet)$ denotes the mth Bessel function. For a pipe partially filled with water, the non-axisymmetric acoustic modes may split and introduce complexity for the post-processing of acoustic data [17]. If the pipe is dry, then the eigen-number k_{mn} in Eq. (2) can be obtained from the zero-velocity condition imposed on the rigid wall of the pipe [15]:

$$J'_{\text{m}}(k_{mn}r)|_{r=R} = 0, \tag{3}$$

where R is the pipe radius. In the above equation ′ denotes partial derivative with respect to r. z-axis wavenumber γ_{mn} in Eq. (1) is given by [15]:

$$\gamma_{mn} = \sqrt{k_0^2 - k_{mn}^2}, \tag{4}$$

where k_0 is the wavenumber in a free space ($k_0 = \omega/c_0$, c_0 is sound speed in air).

Eq. (4) predicts the wavenumber of the mode (m, n) at different frequencies propagating in the pipe. It is clear that γ_{mn} is frequency dependent, i.e., acoustic propagation of these modes (except in the case of plane wave when $k_{00} = 0$) is dispersive. If the free field wavenumber k_0 is larger than the eigen-number, k_{mn}, or the frequency is above the corresponding eigen-frequency, $f_{mn} = k_{mn}c_0/(2\pi)$, then a particular acoustic mode can propagate along the pipe with relatively little attenuation at a phase velocity that is dispersive. Fig. 2 shows schematically the angular and radial dependence of the first four mode shapes in the cylindrical pipe. In this figure the plus or minus correspond to the sign the mode shape function, φ_{mn}, takes for a given values of θ and r in Eq. (1).

2.2. Beamformer for plane wave and higher modes

For an acoustic sensing system with a fixed source and several receiver points collocated in the pipe (see Fig. 3), the acoustic response for the plane wave mode ($\gamma_{mn} = k_0$ in Eq. (1)) received by the jth microphone can be expressed as:

$$p_j(\omega) = \sum_{q=-Q}^{Q} A_{00}(\omega) e^{-ik_0\left[2|z_q| - \text{sgn}(z_q)(jd - d_s)\right]} s^{(0)}(z_q) + \varkappa(\omega), j = 0, 1, \cdots, J \tag{5}$$

where z_0 is the coordinate of the robot (more specifically the speaker's position) is assumed as zero, i.e. $z_0 = 0$, and $\text{sgn}(z_q)$ denotes the sign of z_q. In Eq. (5) z_q is the discrete axial coordinates and Q is the maximum number of axial coordinates. The spatial resolution of this method, z_q, is dependent on the time step, $\Delta t = 1/f_s$, i.e. how fast the reflected acoustic signal is sampled because $z_q = c_0 t_q$, where $t_q = q\Delta t$ is the qth time sampling interval and f_s is the sampling frequency used for data acquisition. The other variables in Eq. (5) are the spacing in the microphone array, d, distance between the first microphone and the speaker, d_s, index of the microphone in the array, j, (see Fig. 3) and the total number of the microphones, J. $s^{(0)}(z_q)$ is the amplitude of the reflection from the artefact located at the position z_q, which can be understood as the reflection coefficient but modulated by the frequency response of the speaker. The superscript index denotes the wave mode order: e.g. $^{(0)}$ denotes the plane wave mode whereas $^{(1)}$ in the following equations denotes the first non-axisymmetric mode. The amplitude of the source related to the reflected plane wave mode is accounted for with $s^{(0)}(z_q)$. When there are no artefacts at z_q, $s^{(0)}(z_q)$ is equal to zero. Therefore, an artefact can be described with an amplitude vector $\mathbf{s}^{(0)} = \{s_1, \cdots, s_Q\}$ that is a sparse vector with many zeroes due to the sparse nature of the artefacts in a pipe [6,7], e.g. the pipe with four artefacts shown in Fig. 3 contains the following artefacts: (i) manhole; (ii) lateral connection; (iii)
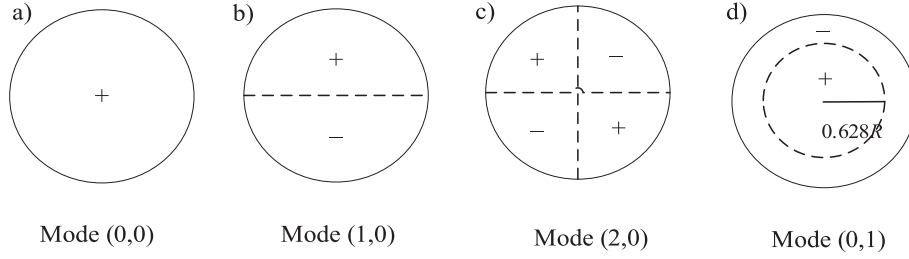
Fig. 2. An illustration of the behavior of the first 4 modal shapes in the cylindrical pipe. Dashed lines are nodal lines for each mode.
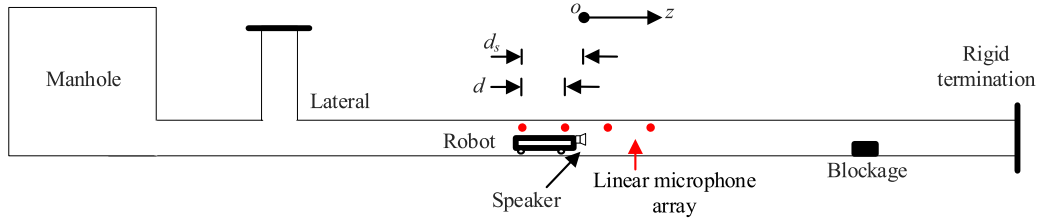

Fig. 3. An illustration of an inspection robot with a linear 4-microphone array arranged axially in a pipe with various artefacts.

blockage; and (iv) rigid termination. In Eq. (5) $n(\omega)$ denotes the noise signal present in the pipe and $A_{00}(\omega)$ is the spectrum of the excitation signal in the plane wave mode (usually a chirp [6,7]). The work by Yu et al [6,7] used a speaker placed at the centre of the cross-section. With this arrangement below the cut-off frequency of the first axisymmetric mode only the plane wave can be excited by the speaker. In this way the complexity of the acoustic field in the pipe is reduced. The phase lag term in the exponent $e^{-ik_0[2|z_q|-\mathrm{sgn}(z_q)(jd-d_s)]}$ uses twice the distance between the robot and the artefacts because the wave propagates from the robot to the artefact and back. The phase lag due to the axially positioned microphone array is also accounted for by this term.

In order to estimate the location of the artefacts in the pipe, Eq. (5) can be solved as an acoustic inverse problem, which can be written as matrices in the discrete frequency domain:

$$\mathbf{p}_j = \mathbf{H}_j^{(0)}\mathbf{s}^{(0)} + n \rightarrow \left\{ \begin{array}{c} p_{j,0} \\ p_{j,1} \\ \vdots \\ p_{j,L} \end{array} \right\}$$

$$= \begin{bmatrix} H_{j,1,-Q}^{(0)} & H_{j,1,1-Q}^{(0)} & \cdots & H_{j,1,Q}^{(0)} \\ H_{j,2,-Q}^{(0)} & H_{j,2,1-Q}^{(0)} & \cdots & H_{j,2,Q}^{(0)} \\ \vdots & \vdots & \ddots & \vdots \\ H_{j,L,-Q}^{(0)} & H_{j,L,1-Q}^{(0)} & \cdots & H_{j,L,Q}^{(0)} \end{bmatrix} \left\{ \begin{array}{c} s_{-Q}^{(0)} \\ s_{1-Q}^{(0)} \\ \vdots \\ s_Q^{(0)} \end{array} \right\} + \left\{ \begin{array}{c} n_1 \\ n_2 \\ \vdots \\ n_L \end{array} \right\} \quad (6)$$

where $H_{j,l,q}^{(0)} = A_{00}(l\Delta f)e^{-ik_0(l\Delta f)[2|qc_0\Delta t|-\mathrm{sgn}(q)(jd-d_s)]}$. Δf is the frequency domain resolution of the discrete Fourier transform used to calculate the acoustic response spectrum in Eq. (5), l and q are the indices of the frequency and distance points, respectively, L and $2Q$ are the total numbers of the frequency and distance points, respectively. When L is larger than $2Q$, the inverse problem of Eq. (6) is over-determined and can be solved using the Least Square (LS) method, e.g. LSQR algorithm [18].

Eqs. (5)-(6) are only defined for the plane wave regime ($f < f_{10}$). Above the first cut-off frequency (f_{10}) of the first non-axisymmetric mode, multiple modes propagate in the pipe shown in Fig. 3 even for the case of speaker placed at the center of the pipe cross-section, causing

wave dispersion and presenting a challenge for signal processing with traditional beamforming methods [8]. In the frequency range $f_{10} < f < f_{20}$ and in the case of an incident plane wave only, both the plane wave and the first non-axisymmetric mode can be excited in the reflected acoustic field. Therefore, using Eq. (1) and superposing the plane wave and the first non-axisymmetric mode one can express the acoustic response as:

$$p_j(\omega) = \sum_{q=-Q}^{Q} A_{00}(\omega)e^{-ik_0[2|z_q|-\mathrm{sgn}(z_q)(jd-d_s)]}s^{(0)}(z_q)$$

$$+ \sum_{q=-Q}^{Q} A_{00}(\omega)e^{-ik_0|z_q|-i\gamma_{10}[|z_q|-\mathrm{sgn}(z_q)(jd-d_s)]}s^{(1)}(z_q) + n(\omega) \quad (7)$$

where $\gamma_{10} = \sqrt{k_0^2 - k_{10}^2}$ ($k_{10} = \frac{1.841}{R}$ and introduced in Eq. (4)), is the wavenumber of the first non-axisymmetric mode. The first sum in Eq. (7) defines solution for the plane wave propagating from the robot to an artefact and reflecting back to the robot as a plane wave mode. The second sum defines the solution for the plane wave propagating from the robot to an artefact and reflecting back to the robot as the first non-axisymmetric mode. As before, $s^{(0)}(z_q)$ and $s^{(1)}(z_q)$ denote the reflection amplitude of the plane wave and the first non-axisymmetric mode, respectively. Remaining components of the scattered wave field in the frequency range $f_{10} < f < f_{20}$, i.e. first-mode propagation and plane/first-mode reflection, are assumed to be of order much smaller than those in Eq. (7) since the speaker is placed in the center of the pipe cross-section (nodal position of mode (1,0) as shown in Fig. 2). There are multiple transmission/reflection paths supported by pipe geometry, e.g. sound wave emitted from the robot, transmitted through a lateral connection or joints, reflected from a further placed blockage, then received and scattered by the robot. In this case, it is assumed that the plane wave propagation from the robot to the artefact, and the plane wave and the first-mode reflections are dominant contributors to the overall acoustic field received by the microphone array. To the best of our knowledge this idea has not ever been tested in a pipe environment where the acoustic field is strongly multimodal.

Similarly to Eq. (6), Eq. (7) can also be written in a vectorized form:

$$\mathbf{p}_j = \mathbf{H}_j\mathbf{s} + n_j \rightarrow \mathbf{p}_j = \begin{bmatrix} \mathbf{H}_j^{(0)} & \mathbf{H}_j^{(1)} \end{bmatrix} \begin{bmatrix} \mathbf{s}^{(0)} \\ \mathbf{s}^{(1)} \end{bmatrix} + n_j \quad (8)$$

where $\mathbf{p}_j = \begin{bmatrix} p_{j,1} & \cdots & p_{j,L} \end{bmatrix}^T$,

$$\mathbf{H}_j = \left[\mathbf{H}_j^{(0)} \mathbf{H}_j^{(1)}\right]$$

$$= \begin{bmatrix} H_{j,1,-Q}^{(0)} & H_{j,1,1-Q}^{(0)} & \cdots & H_{j,1,Q}^{(0)} & H_{j,1,-Q}^{(1)} & H_{j,1,1-Q}^{(1)} & \cdots & H_{j,1,Q}^{(1)} \\ H_{j,2,-Q}^{(0)} & H_{j,2,1-Q}^{(0)} & \cdots & H_{j,2,Q}^{(0)} & H_{j,2,-Q}^{(1)} & H_{j,2,1-Q}^{(1)} & \cdots & H_{j,2,Q}^{(1)} \\ \vdots & \vdots & \ddots & \vdots & \vdots & \vdots & \ddots & \vdots \\ H_{j,L,-Q}^{(0)} & H_{j,L,1-Q}^{(0)} & \cdots & H_{j,L,Q}^{(0)} & H_{j,L,-Q}^{(1)} & H_{j,L,1-Q}^{(1)} & \cdots & H_{j,L,Q}^{(1)} \end{bmatrix}$$

$$\mathbf{s} = \begin{bmatrix} \mathbf{s}^{(0)} \\ \mathbf{s}^{(1)} \end{bmatrix} = \begin{bmatrix} s_{-Q}^{(0)} & s_{1-Q}^{(0)} & \cdots & s_Q^{(0)} & s_{-Q}^{(1)} & s_{1-Q}^{(1)} & \cdots & s_Q^{(1)} \end{bmatrix}^T$$

$$\mathbf{n}_j = \begin{bmatrix} n_{j,1} & n_{j,2} & \cdots & n_{j,L} \end{bmatrix}^T$$

with $H_{j,l,q}^{(0)} = A_{00}(l\Delta f)e^{-ik_0(l\Delta f)\left[2|qc_0\Delta t|-\mathrm{sgn}(z_q)(jd-d_s)\right]}$,

$$H_{j,l,q}^{(1)} = A_{00}(l\Delta f)e^{-ik_0|qc_0\Delta t|-i\gamma_{10}\left[|qc_0\Delta t|-\mathrm{sgn}(z_q)(jd-d_s)\right]}$$

For a linear microphone array with J elements, the acoustic data from these sensors can be fused by combining Eqs. (6) and (8) in the following form:

$$\mathbf{p} = \mathbf{Hs} + \mathbf{n} \rightarrow \begin{Bmatrix} \mathbf{p}_0 \\ \mathbf{p}_1 \\ \vdots \\ \mathbf{p}_J \end{Bmatrix} = \begin{bmatrix} \mathbf{H}_0 \\ \mathbf{H}_1 \\ \vdots \\ \mathbf{H}_J \end{bmatrix} \mathbf{s} + \mathbf{n} \tag{9}$$

It is assumed that the acoustic artefacts have limited extent spatially, so that the vector $\mathbf{s}$ has sufficient sparsity. The sparse nature of the artefacts (e.g. blockages/junctions/pipe ends) is common in drainage and wastewater pipes. It has been illustrated in Ref. [11,6,7] that the sparsity of impulse response in the pipe can be observed in the time domain and wavelet domain. As discussed in Ref. [6], the sparse representation using wavelet basis functions can reduce the background noise and some higher-order modal components in the impulse response without cancelling the acoustic features from artefacts. Similarly, this paper makes uses of the frequency domain sparsity of the artefact's amplitude $\mathbf{s}$ in Eq. (9).

The sparsest solution $\widehat{s}$ satisfies the following optimization problem [19]:

$$\widehat{\mathbf{s}} = \underset{\mathbf{s}}{\mathrm{argmin}} \|\mathbf{s}\|_0 \quad \text{subject to } \mathbf{Hs} - \mathbf{p} = 0 \tag{10}$$

where $\|.\|_0$ denotes the ℓ_0 pseudo-norm, which is the number of the non-zero components of the vector. This is also referred to as the cardinality of $\mathbf{s}$ [19]. The optimization problem in Eq. (10) is non-convex and its solution is usually found by using a brute-force search [19] which can be computationally expensive. Fortunately, it is possible to relax the optimization in Eq. (10) to a convex ℓ_1-minimization [19]:

$$\widehat{\mathbf{s}} = \underset{\mathbf{s}}{\mathrm{argmin}} \|\mathbf{s}\|_1 \text{ subject to } \mathbf{Hs} - \mathbf{p} = 0 \tag{11}$$

where $\|.\|_1$ denotes the l_1-norm, which describes the sum of absolute values of the vector $\mathbf{s}$.

A related convex optimization problem is the following:

$$\widehat{\mathbf{s}} = \arg\underset{\mathbf{s}}{\min}\left\{\|\mathbf{Hs} - \mathbf{p}\|_2^2 + \lambda\|\mathbf{s}\|_1\right\} \tag{12}$$

where $\lambda > 0$ is a regularisation parameter that weights the importance of sparsity. In this paper the ℓ_1-norm regularization is solved using the Sparse Reconstruction by Separable Approximation (SpaRSA) algorithm [20] (see details in the Appendix A). After estimating the amplitude vector $\widehat{s}$, the location of the artefacts can be obtained directly by searching for the non-zero components s_q at the corresponding axial

coordinates $\underline{z}_q$.

2.3. LCMV beamformer

For comparison, a time-domain broad-band Linearly Constraint Minimum Variance (LCMV) beamformer [21] was used in this work. The LCMV beamformer represents a sophisticated approach in the field of acoustic signal processing, aimed at enhancing signal reception from a specific direction while simultaneously suppressing interference and noise from other directions [21,8]. This technique is particularly effective in applications requiring spatial filtering, such as sonar, radar and telecommunications, to improve signal clarity and quality [8]. Consequently, acoustic beamforming proves to be instrumental in the context of acoustic sensing in pipes to discriminate echoes originating either from the front or behind the robotic sensor. This capability significantly enhances the precision and accuracy in localizing features within the pipe, thereby improving the effectiveness of diagnostic and navigational tasks conducted within such environments.

The core principle of the LCMV beamformer is to minimize the output power of the beamformer under certain linear constraints. These constraints ensure that the signal from the desired direction is passed through without attenuation, while signals from other directions are attenuated. The optimization problem can be formulated as follows [21]:

$$J(\mathbf{w}) = \underset{\mathbf{w}}{\min} \ \mathbf{w}^H\mathbf{R_p}\mathbf{w} \quad \text{subject to } K \text{ linear constraints} \quad \mathbf{C}^H\mathbf{w} = \mathbf{f} \tag{13}$$

where $J(\mathbf{w})$ is the cost function representing the output power of the beamformer, $<\bullet>^H$ denoting Hermitian (conjugate transpose), $\mathbf{w}$ is the estimated weights applied to the array inputs, i.e. microphone signals, $\mathbf{C}$ is the constraint matrix which contains K steering vectors directing the beamformer to preserve the signal from the desired direction, $\mathbf{f}$ is the constraint vector, specifying the response of the beamformer in the direction of interest, $\mathbf{R_p} = E[\mathbf{pp}^H]$ is the correlation matrix of the received signals.

The solution of the beamformer is given by [21]:

$$\mathbf{w}_{\text{LCMV}} = \mathbf{R_p^{-1}}\mathbf{C}\left(\mathbf{C}^H\mathbf{R_p^{-1}}\mathbf{C}\right)^{-1}\mathbf{f} \tag{14}$$

This results in a directional beam pattern that can adaptively focus on the signal of interest while nullifying unwanted signals, thus enhancing the overall signal-to-noise ratio (SNR) and improving the quality of signal reception. In this paper, the solution of broadband LCMV beamformer was obtained by using the function in Matlab: @ *phased.TimeDelayLCMVBeamformer* [22,23,24].

It should be noted that the LCMV beamformer is derived for plane wave fields, a characteristic which inherently constrains its applicability in waveguides (i.e. pipes), where the acoustic waves regularly exhibit dispersive properties. Consequently, the methodology introduced in Section 2.2 (Eqs. (7) and (8)) is tailored to pipe environments accommodating the dispersive nature of acoustic waves in such settings.

3. Experimental setup

The experimental setup used two cases of PVC pipe network (see Fig. 4): (i) a straight section of a 21.5 m long 150 mm diameter pipe with a manhole at one end; (ii) a straight section of a 20.83 m long 150 mm diameter main pipe with a manhole at one end, a 100 mm diameter 1.91 m long lateral connection attached at 90° 9.41 m away from the manhole, and a blockage at 6.39 m from the lateral connection. This blockage was made from concrete, which provided a 40 % blockage ratio (blockage hight divided by the pipe diameter) and was 150 mm long. The blockage was placed in the pipe network case (ii) as shown in Fig. 4(b) to validate the performance of the proposed algorithm for separating overlapped acoustic echoes from blockage lateral or manholes. The straight section was terminated with a heavy wooden board
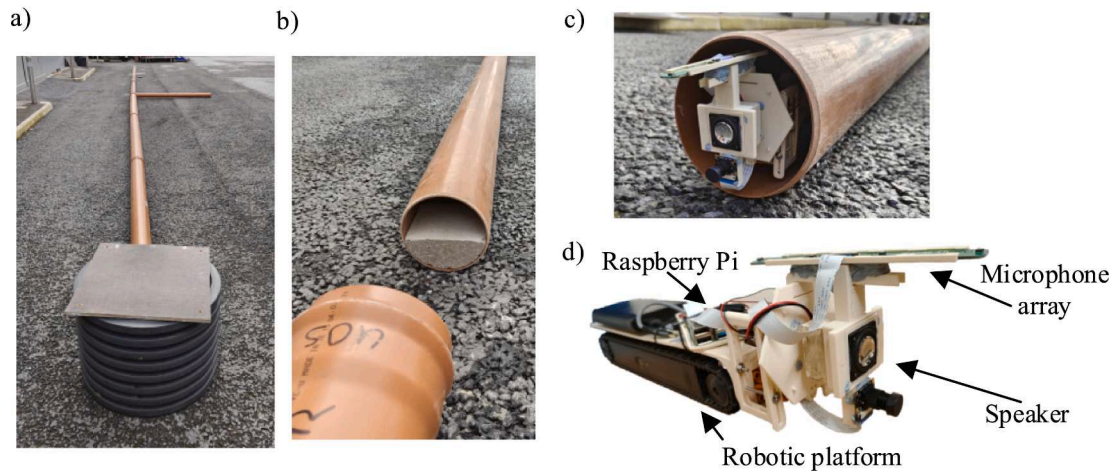
Fig. 4. (a) The pipe network layout with a manhole and a lateral connection; (b) the 40 % concrete blockage in the pipe; (c) the Looj iRobot in a pipe; (d) the complete robotic sensing platform with a 4-microphone array and speaker.

at one end and manhole at the other end (see Fig. 4 (a)). The density of PVC pipes is around 1300 kg/m^3, i.e. two orders of magnitude greater than that of air. Therefore, the pipe wall was assumed to be acoustically rigid.

The acoustic sensing system was mounted on a remotely controlled robot (iRobot Looj 330 by iRobot [22], around 400 mm long and 73 mm wide) that was moved at a velocity of around 0.1 m/s (see Fig. 4(c) and (d)). Acoustic sensors used in this work consisted of a loudspeaker and four-microphone linear array. The acoustic and data acquisition setup included an array, speaker, Raspberry Pi 4 serving as the processor, power amplifier for the speaker, ADC (Analog-to-Digital Converter) and DAC (Digital-to-Analog Converter) components. The data acquisition was implemented on Raspberry Pi with a Linux OS which simultaneously played and recorded sound. The sampling rate was $f_s = 16$ kHz. A 100 – 3000 Hz sweep sine with duration 10 s was used as the excitation signal.

Signal was pre-processed by the deconvolution method to obtain the impulse response for each microphone:

$$\widetilde{P}_j(t) = \mathscr{F}^{-1}\left\{ \frac{\mathscr{F}\left[P_j(t)\right]}{\mathscr{F}\left[e(t)\right] + \beta} \right\}, j = 0, 1, \cdots, J, \tag{15}$$

where $\mathscr{F}$ and $\mathscr{F}^{-1}$ denote the forward and inverse Fourier transform operator and β is the parameter of regularization ($\beta = 0.1$ in this work). A 4th order Butterworth band-pass filter was used to extract the signal in the frequency range of interest, e.g. 200–1300 Hz for plane wave and 1500–2000 Hz for the first non-axisymmetric mode regime.

The speaker was located at the centre of the pipe within a 5 mm positional mean error initially, although this could have varied slightly due to the robot movement inside the pipe. The microphone array, consisted of 4 omni-directional microphones ($J=4$ in Eq. (5)-(9)) with 50 mm spacing, was set up close to the top of the pipe. This arrangement was to avoid any contact with the water when the robot would be used to inspect a partially filled drainage pipe. The microphone type used in this experiment was MSM321A3729H9CP by MEMSensing Microsystems Co. Ltd. The microphone size was 3.76 mm × 2.95 mm × 1.1 mm. It had –32 dB sensitivity at 1 kHz (ref. 1 V/Pa) providing an estimated 65 dB signal to noise ratio in the frequency range of interest. The Visaton 2242 speaker with the diaphragm of 32 mm in diameter was driven with a 3 W power supply. Its frequency range was 150–2000 Hz.

The number of frequency points in the spectral analysis significantly affects the computation efficiency of the processing. In this paper, the sensing distance was limited within 50 m (i.e. $z_Q = 25$ m, $z_{-Q} = -25$ m). The number of distance points defined as $Q = z_Q/c_0 f_s$ was around 2048 points for $f_s = 16$ kHz.

The localization error (distance between the robot and the pipe feature) was calculated as:

$$\varepsilon = \frac{\left| z_p - z_r \right|}{z_r} \tag{16}$$

where z_p and z_r are the predicted and real locations of the pipe feature, respectively.

4. Experimental results

This section presents a set of experimental results of beamforming algorithm proposed in this paper for the localization of robot and blockage in a pipe network. For underground sewage pipe inspection a robot can be initially placed into the pipe through a manhole access. In the experiment a typical manhole was recreated as shown in Fig. 5(a). Manhole is acoustically reflective and reverberant environment that produces a prolonged impulse response detectable by the robot over long distances in the pipe. As shown schematically in Fig. 5(a), a robot used in the experiment was initially 5.3 m away from the manhole, which was indicated accurately by the acoustic impulse response of the pipe network (see echo from manhole indicated in Fig. 5(b)). However, the reverberant sound wave due to the manhole extends to around 8 m (5–13 m range in the impulse response in Fig. 5(b)) causing a "blind" detection zone. A spatial filtering based on the beamforming technique from Section 2 was used here to separate the echoes from the front or back of the robot, so that the "blind zone" caused by the manhole or any other features at the rear of the robot can be removed or significantly reduced.

As shown in Fig. 5(b), the phase delay from the linear microphone array explicitly indicates the direction of the echoes from the manhole or the pipe end. The multiple reflection has two paths: (i) robot → pipe-end → robot → manhole → robot, and (ii) robot → manhole → robot → pipe-end → robot. It should be noted that both paths can be combined in the analysis and used to reconstruct the length of the whole pipe. The path (i) can be regarded as the echo coming from left of the robot, whereas the path (ii) can be regarded as the echo coming from the right.

Fig. 6(c) illustrates the impact of the first non-axisymmetric mode on the sound reflected by the blockage in the pipe and propagating in the frequency range that includes the first non-axisymmetric mode. This can be compared with the case illustrated in Fig. 6(c) where the incident sound is generated below the cut-off frequency. This mode demonstrates a lower group velocity compared to that of a plane wave, resulting in a phase delay observed in the signal received by the microphone array [7]. The phenomenon of wave dispersion complicates the localization and
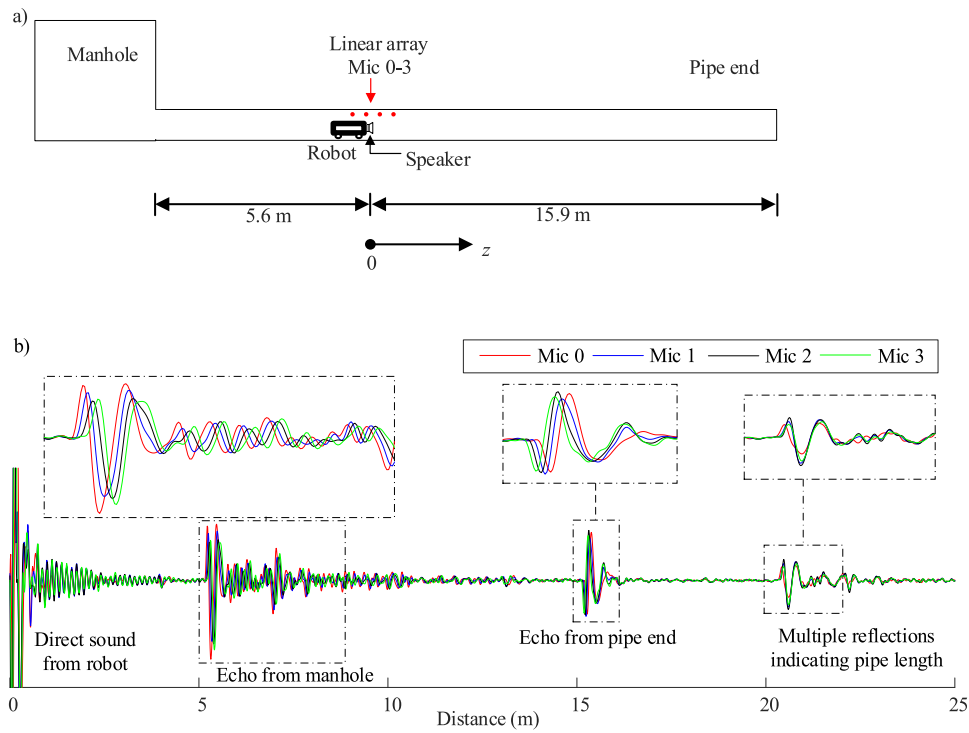
Fig. 5. (a) An impression of the robot with a linear microphone array in the straight pipe with a manhole; (b) the impulse response (frequency range 200–2000 Hz) plotted against the distance propagated by the sound wave ($d = c_0 t / 2$) along the coordinate z.
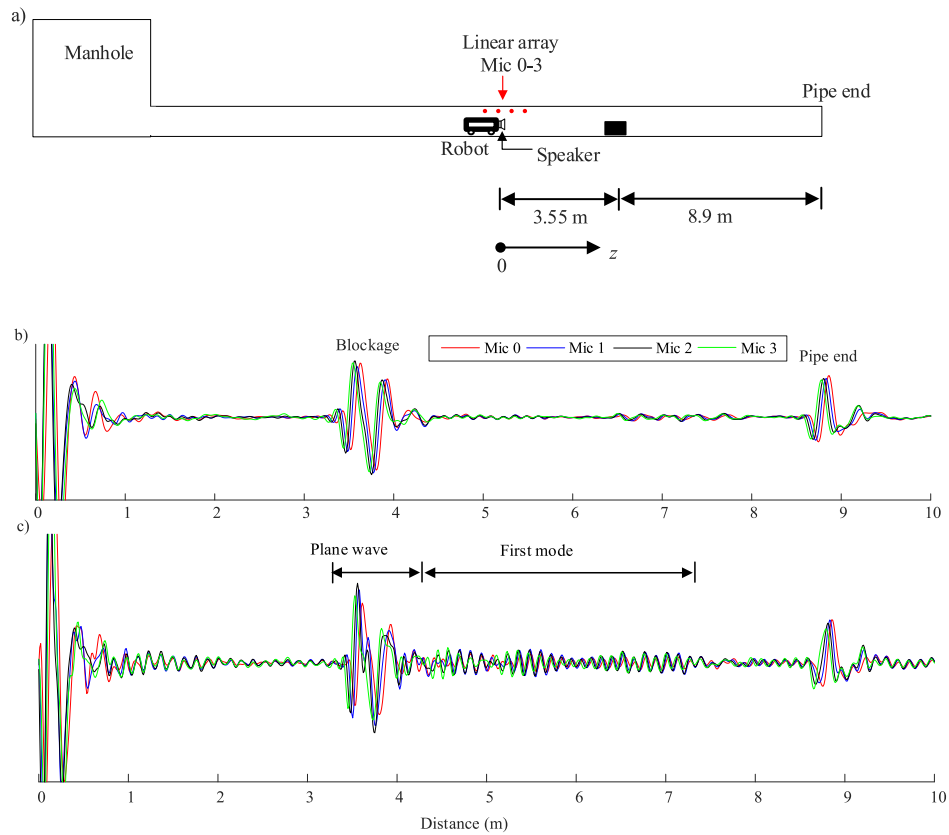

Fig. 6. (a) A robot with a linear microphone array in the straight pipe with a manhole and blockage; (b) the impulse response plotted against the distance propagated by the sound wave ($d = c_0 t / 2$) along the coordinate z in the plane wave regime (frequency range 200–1300 Hz); (c) the impulse response beyond the plane wave regime (frequency range 200–2000 Hz).

detection of pipe conditions, especially when multiple artefacts are positioned in a close proximity (less than 3 m). The overlapping of echoes attributable to wave dispersion and their direction relative to the robotic sensor (either front or rear) presents a significant challenge. Distinguishing and identifying these overlapping echoes represents the principal novelty of this paper.

4.1. Plane wave regime beamformer

Fig. 7 shows the acoustic reflections from both negative (left from the robot) and positive (right from the robot) directions calculated with the proposed beamformer using the experimental setup shown in Fig. 5(a). Contrary to that shown in Fig. 5(b), the reflections depicted in Fig. 7 were arranged along the coordinate axis with the help of the beamforming algorithm (LCMV and the sparse representation) to demonstrate the positive and negative directions and to estimate more accurately the position of the artefact with respect to the robot. In the plane wave regime ($f < f_{10}$), the time-delay LCMV beamformer [21] can be used to enhance the reconstruction of reflected acoustic waves originating from the left while supressing those from the right through the specification of the leftward beamforming direction. For example, while the robot was at 4.07 m, the amplitude of the manhole reflected signal at negative co-ordinates from −7 m to −4 m was significantly higher than its counterpart at positive coordinates from 4 m to 7 m. Similar results can be observed when the robot was at other locations as shown in Fig. 7. This indicates the functionality of the LCMV beamformer, although the LCMV beamforming does not fully cancel the echoes from the manhole.

The same procedure was implemented for the rightward reflections from the pipe end, where the residue of the leftward echoes from the manhole can be also observed (see Fig. 7). Whereas the sparse representation beamformer (Eqs. (6) and (9)) presents a better spatial filtering results with almost ideally cancelled manhole echoes in the signals arriving from the right (see Fig. 7). This enables us to distinctly separate the acoustic reflections with respect to the rear or front side of the robot into negative and positive coordinates. Such differentiation can be used for the precise localization and mapping of the conditions in the pipe and for the robot's navigation.

The reverberant signal due to the presence of the manhole on the left was also significantly cancelled. As shown in Fig. 7, the echo signal from the manhole only lasted for 2.5 m compared to 8 m range in the impulse response recorded without beamforming algorithm SRB (see Fig. 5(b), manhole reflections).
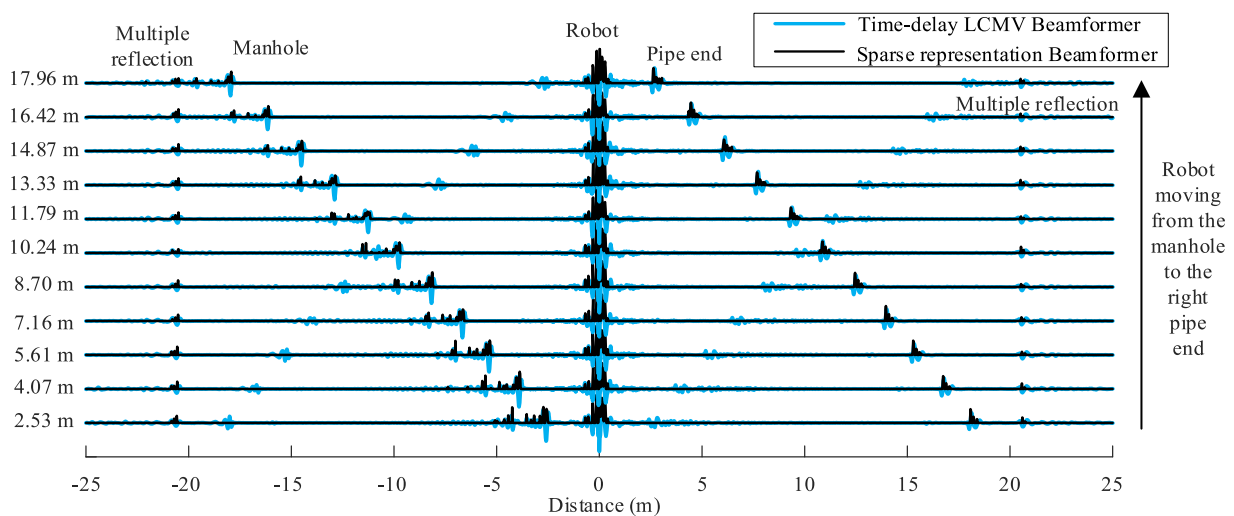
Fig. 8(a) shows schematically a more complicated pipe network with a manhole, lateral connection (at the right side of the robot as shown in Fig. 4(a)) and a blockage used in the experiment with the beamforming algorithms. The results of this experiment are presented in Fig. 8(b). Again, the proposed sparse representation algorithm strongly cancels the rightward echoes with leftward focusing beamforming and results in a significantly better spatial filtering compared to the time-delay LCMV beamformer. The same phenomenon can be observed for rightward echoes.

As shown in Fig. 8(b), the spatial extend of the echo signal from the manhole is around 2.5 m. This is significantly reduced in comparison with the 8 m interval in the impulse response without beamforming (see Fig. 5(b)). Additionally, the reflection from the manhole can be identified at the back direction (negative distance in Fig. 5(b)), so that the acoustic feature from the front of the robot can be separated.

Fig. 8(b) also shows that the proposed algorithm can separate the reflections from left and right when the robot is positioned between two pipe conditions, e.g. when it is between the manhole and lateral (e.g. robot at 4.88 m), or manhole and blockage (e.g. robot at 7.77 m). The proposed beamformer can be used to detect the reflection from the two directions. This cannot be achieved by using a mono receiver [11] or circular sensor array placed in the same cross-section on a static robot [6]. The proposed beamforming algorithms enables us to localize the pipe features within 3 % of the true distance to a reflecting feature in the pipe.

4.2. First non-axisymmetric mode regime beamformer

Beyond the first cut-off frequency ($f > f_{10}$) it is possible to use the acoustic scattering properties of the blockage and lateral connection to discriminate between them and to extract the reflections from a particular artefact. Within the frequency range $f_{10} < f < f_{20}$, there are two different acoustic wave modes that can propagate in the pipe: plane wave and the first-non-axisymmetric mode. The reflection coefficient of the plane wave scattered by the lateral connection beyond the first cut-off frequency f_{10} is well below 0.1 which is significantly smaller than that for the 40 % blockage (>0.2) as discussed in Ref. [6].

According to [7], the first non-axisymmetric wave mode reflected from the left/right branch lateral connection due to a plane wave excitation has a vertical nodal line, whereas its reflection from the blockage at the bottom of the pipe has a horizontal nodal line (see Fig. 2(b)). In Ref. [7], a circular array was used to analyze the first non-axisymmetric

Fig. 7. Spatially filtered impulse responses in the plane wave regime (frequency range 200–1300 Hz) using time-delay LCMV beamformer (blue curves) and the absolute value of the sparse amplitude vector for plane wave components $|\hat{s}^{(0)}|$ of Eq. (6) (black curves). Each set of data shown corresponds to the *z*-axis coordinate of the robot between 2.53 m and 17.96 m.
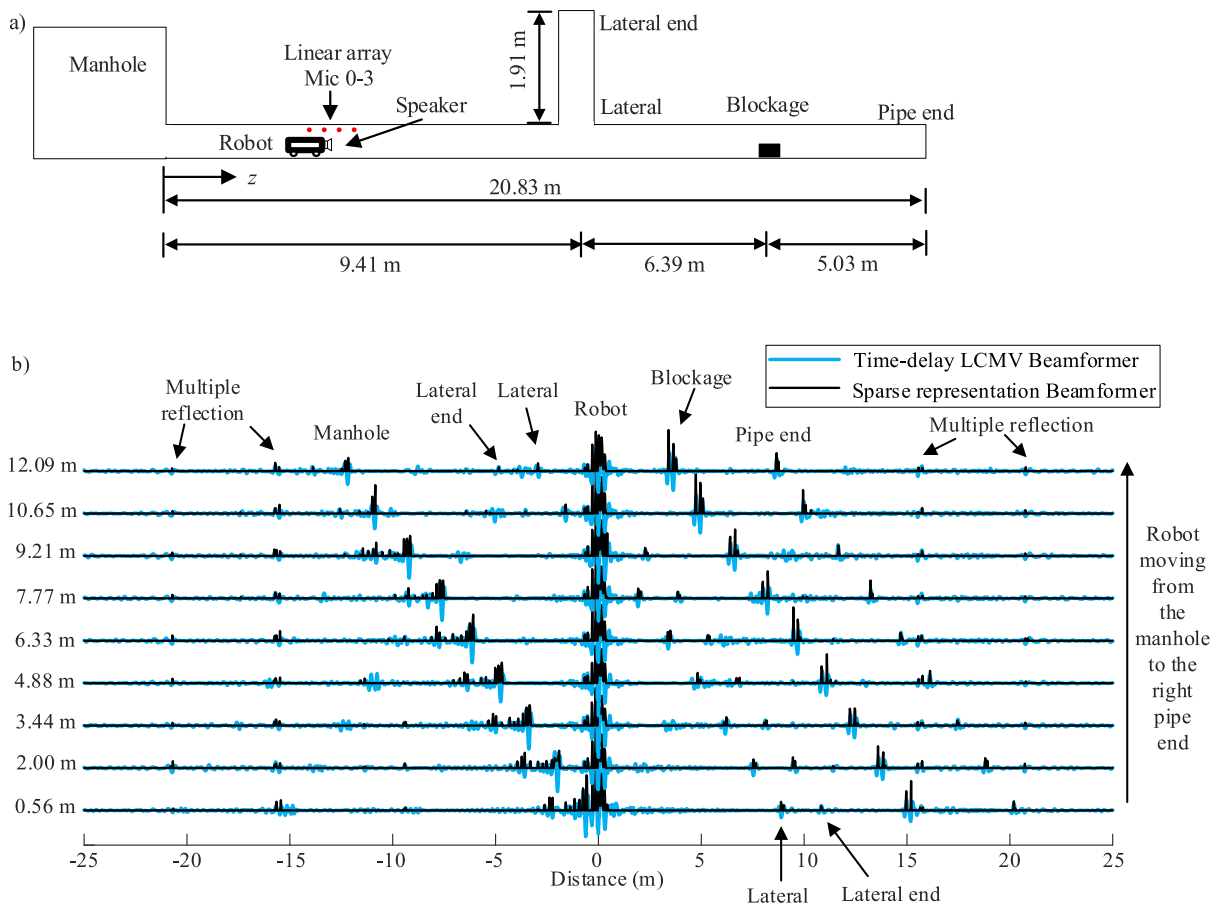
Fig. 8. (a) A robot with a linear microphone array in a pipe with a manhole, lateral connection, and a blockage; (b) spatially filtered impulse response (frequency range 200–1300 Hz) using time-delay LCMV beamformer (blue curves) and the absolute value of the sparse amplitude vector for plane wave components $\left|\hat{s}^{(0)}\right|$ of Eq. (6) (black curves). Each set of data shown corresponds to the *z*-axis coordinate of the robot between 0.56 m to 12.09 m.

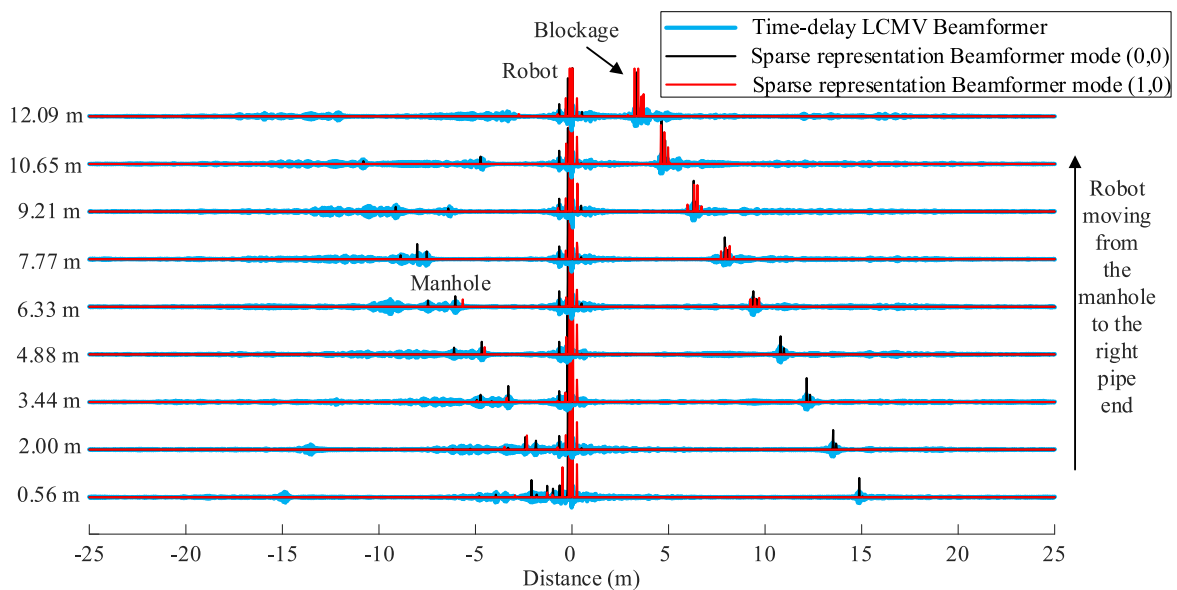**Fig. 9.** Spatially filtered impulse responses (frequency range 1500–2000 Hz) using time-delay LCMV beamformer (blue curves). The absolute value of the sparse amplitude vector for plane wave components $\left|\hat{s}^{(0)}\right|$ of Eq. (8) (black curves); the absolute value of the sparse amplitude vector for the first non-axisymmetric mode wave components $\left|\hat{s}^{(1)}\right|$ of Eq. (8) (red curves).

mode for the circumferential localization of the pipe defects. This paper extends the previous work using a linear array to focus on the localization of blockage. In this work, the microphone array is positioned at the top of the cross-section of the pipe, as shown in Fig. 4(d), which is the nodal line of the first non-axisymmetric mode of the reflection from the lateral connection. Therefore, the effect of the first non-axisymmetric mode caused by the lateral reflection is minimised, while the reflection from the blockage can be effectively measured.

Hence, the acoustic signature of a more concerning feature, i.e. blockage, can be extracted for detection and localization. This non-axisymmetric mode method was tested with the robotic sensing setup in the pipe network as shown in Fig. 8(a) and Fig. 4(a). Fig. 9 shows that in the frequency range $f_{10} < f < f_{20}$ the reflection from the lateral connection is minimized and the blockage signature is enhanced with the time-delay LCMV beamformer technique and proposed sparse representation algorithm. By solving Eqs. (8), (9) and (12), the algorithm shows an improved spatial filtering performance compared to the time-delay LCMV beamformer technique, particularly at the positive coordinates where the reflections from the manhole have been cancelled. With the modal decomposition, the reflection amplitude of both the plane and the first non-axisymmetric mode are clustered at almost the same coordinate indicating the location of the blockage. It is also noted that the amplitude of the first non-axisymmetric mode increases significantly when the robot is approaching the blockage.

4.3. Length of the pipe section

Estimation of the length of the pipe is important for the localization and mapping of pipe network. As shown in Fig. 7 and Fig. 8, the multiple reflections measured at various robot locations in the plane wave regime consistently indicate the pipe length. Therefore, the multiple reflections in the plane wave regime can be used to estimate the length of the pipe [11]. However, this method requires the sequential measurements from the robot as it moves which increases the complexity of the algorithm of robotic autonomous control and increases unnecessarily the time required for robot to traverse the inspected length of the pipe [11].

With the proposed beamformer algorithm the length of the pipe can be estimated with a single measurement. As shown in Fig. 7(b) and Fig. 8 (b), multiple reflections in the positive and negative directions appear in the same spatial interval with respect to the robot's position at $z = 0$. The measure of the pipe length can then be expressed as:

$$\mathbf{L}_{p1} = |\widehat{\mathbf{s}}(z_{-q})|^{\circ}|\widehat{\mathbf{s}}(z_q)| = |\widehat{s}_0 \quad \widehat{s}_{-1} \quad \cdots \widehat{s}_{-Q}|^{\circ}|\widehat{s}_0 \quad \widehat{s}_1 \quad \cdots \widehat{s}_Q| \qquad (17)$$

where $^{\circ}$ denotes the Hadamard product (elementwise multiplication) of two arrays $|\widehat{\mathbf{s}}(z_{-q})|$ (the reflection amplitudes associated with the negative coordinates) and $|\widehat{\mathbf{s}}(z_q)|$ (the reflection amplitudes associated with the positive coordinates). Since both $|\widehat{\mathbf{s}}(z_{-q})|$ and $|\widehat{\mathbf{s}}(z_q)|$ are sparse vectors, reflection pulses from different positive/negative distances should be cancelled and only reflections having the same positive and negative coordinates give non-zero elements in measure $\mathbf{L}_{p1}$ from Eq. (17).

It should be noted that in case when both echoes appear at the same positive and negative coordinate, they may fail to classify as multiple reflections needed to estimate the true pipe length. For example, when the robot is located at the centre between two features (e.g. when the robot was at 10.24 m in Fig. 7 that corresponds to the middle between the manhole and pipe end), the left and right reflected pulses appear at almost the same distance from the robot, which is about half of the pipe length. Hence, another measure is proposed in this paper.

Since the direction of the echoes has been estimated using the beamforming, the length of the pipe section between the left and right pipe features can be estimated directly by the summation of the distances between two neighbouring echoes. In this paper, a convolution between vectors $\widehat{\mathbf{s}}(z_{-q})$ and $\widehat{\mathbf{s}}(z_q)$ is used as a method to add distances

together resulting in a new measure given by:

$$\mathbf{L}_{p2} = |\widehat{\mathbf{s}}(z_{-q})|^*|\widehat{\mathbf{s}}(z_q)| = |\widehat{s}_0 \quad \widehat{s}_{-1} \quad \cdots \widehat{s}_{-Q}|^*|\widehat{s}_0 \quad \widehat{s}_{-1} \quad \cdots \widehat{s}_{-Q}|, \qquad (18)$$

where * denotes the convolution of two vectors. Since the convolution resulting vector has a length $(2Q+1)$, it is proposed to truncate $\mathbf{L}_{p2}$ vector to $Q+1$ elements so that $\mathbf{L}_{p2}$ has the same length as $\mathbf{L}_{p1}$. Using the product of $\mathbf{L}_{p1}$ and $\mathbf{L}_{p2}$, we propose the measure $\mathbf{L}_p = \mathbf{L}_{p1}{}^{\circ}\mathbf{L}_{p2}$ to estimate the length of the pipe. Note that $\widehat{\mathbf{s}}(z_{-q})$ and $\widehat{\mathbf{s}}(z_q)$ are sparse and reflection pulses may not be continuous as shown in Fig. 7 and Fig. 8. A moving average with a sliding windowing length $K=6$ (refer to 0.06 m distance windowing) is suggested in this work to smooth the vectors $\widehat{\mathbf{s}}(z_{-q})$ and $\widehat{\mathbf{s}}(z_q)$ maintaining relatively narrow width of the pulses. Fig. 10 shows the result of the sparse amplitude vector before and after the moving average process over the frequency range of 200–1300 Hz. It is worth noting that when the sliding windowing length of the moving average is too small (e.g. less than 5), the smoothness of the sparse amplitude vector may not be sufficient for post-processing. When the sliding windowing length is too large (e.g. greater than 10), the peak identifying the distance the pipe section may become too wide, resulting in the false identification of the pipe length. It is found that the sliding windowing length can be chosen between 6–10 points (refer to 0.06–0.1 m distance windowing) in this paper. The proposed algorithm $\mathbf{L}_p$ for the prediction of the pipe length combining the two measures $\mathbf{L}_{p1}$ and $\mathbf{L}_{p2}$ is shown in Table 1.

Fig. 11 and Fig. 12 shows the estimations of the length of the pipe, $\mathbf{L}_p$, $\mathbf{L}_{p1}$ and $\mathbf{L}_{p2}$, obtained using the algorithm detailed in Table 1 over the frequency range 200–1300 Hz when the robot was located in the pipe section between the manhole and lateral connection (see Fig. 11(a)). The proposed algorithm can be used to estimate the lengths of the following four pipe sections: (d_1) manhole-lateral; (d_2) manhole-lateral end (see Fig. 11(a)); (d_3) manhole-blockage; and (d_4) manhole-pipe end. As shown in Fig. 11(b) the measure $\mathbf{L}_p$ that combines both $\mathbf{L}_{p1}$ and $\mathbf{L}_{p2}$ can accurately estimate the lengths of the pipe sections with (d_1) 9.52 m, (d_2) 11.43 m, (d_3) 15.8 m, and (d_4) 20.82 m. The results are within 2 % of the true length. The $\mathbf{L}_{p1}$ measure only uses the information of the multiple reflections and, as a result, wrongly classifies distances when the robot is located in the middle of manhole-lateral (d_1) and manhole-lateral end (d_2) sections.

The coordinates of the peaks within the measure $\mathbf{L}_{p2}$ signify the length of the pipe, aligning with the measurement results obtained from $\mathbf{L}_p$. Additionally, there are peaks of relatively lower amplitude, which can be ascribed to the reverberation effects of the manhole convoluted with reflections from other reflections of the pipe features. To diminish the cases of wrongly predicted pipe's length and to enhance the prediction's resilience against interferences from noise and manhole reverberation, a threshold for $\mathbf{L}_p$ was established at 10^{-3}.

When the robot was located between the lateral and blockage the section lengths corresponded to: lateral-blockage (d_1); manhole-blockage (d_2); and manhole-pipe end (d_3). Using the measure $\mathbf{L}_p$ these section lengths were estimated as $d_1 = 6.5$ m, $d_2 = 15.78$ m and $d_3 = 20.79$ m within less than 2 % of the true lengths. Note that when the robot was between the lateral and the blockage, the robot body reduced the amplitude of the reflection from the left of the pipe since the sensors were facing in the right direction. Therefore, multiple reflection between the lateral connection end and the blockage were identified with small amplitude of $\mathbf{L}_p$.

5. Conclusions

This study has proposed and successfully validated a novel beamforming technique for the localization of artefacts in a pipe and for the estimation of the length of the pipe sections. The proposed technique is based on sparse representation of the acoustic signals recorded on a compact linear microphone array mounted on a static robotic platform.
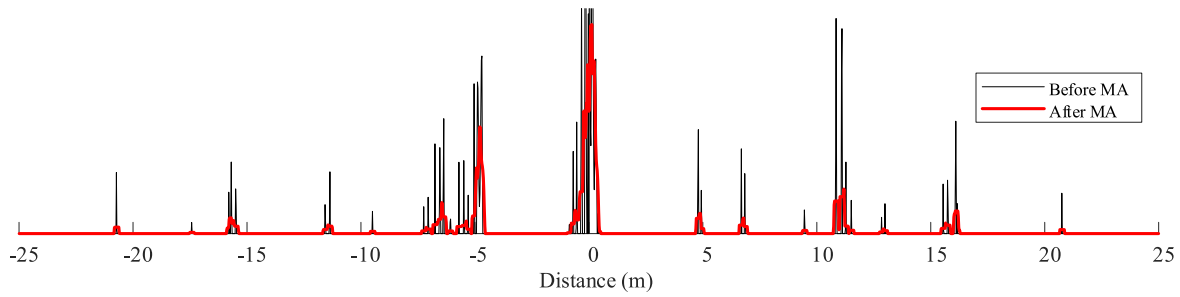
Fig. 10. An example of the absolute value of a sparse amplitude vector $|\hat{s}|$ before moving average (black curve) and after moving average (red curve) is applied.

Table 1
Algorithm 2 – Pipe length estimation.

Task: To estimate the length of the pipe
Input: Reflection amplitude results from Eq. (9): $\left|\hat{s}(z_{-q})\right|$ and $\left|\hat{s}(z_q)\right|$
Steps:
    1. Moving average of $\hat{s}(z_{-q})$ and $\hat{s}(z_q)$ with a sliding length K ($K = 5$ in this paper) gives $\hat{s}_{MA}(z_{-q})$ and $\hat{s}_{MA}(z_q)$.
    2. Calculate the first measure: $L_{p1} = \hat{s}_{MA}(z_{-q}) \circ \hat{s}_{MA}(z_q)$
    3. Calculate the second measure: $L_{p2} = \hat{s}_{MA}(z_{-q}) * \hat{s}_{MA}(z_q)$
    4. Calculate the final measure: $L_p = L_{p1} \circ L_{p2}$
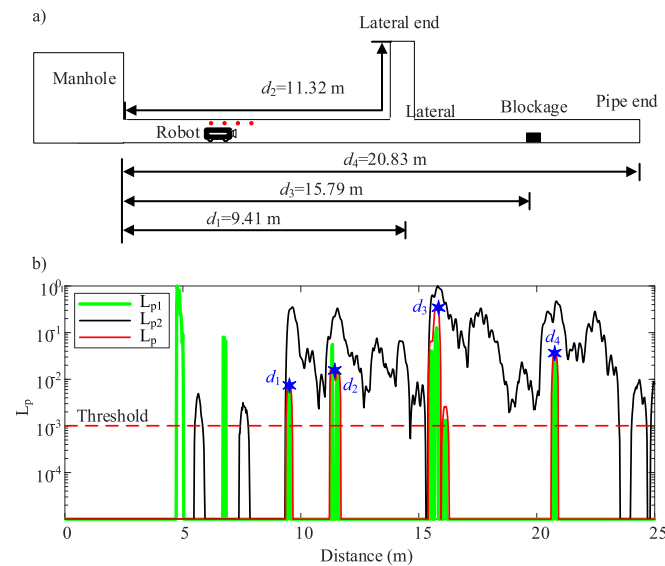Output: L_p.

Fig. 11. The estimations of the pipe section length: (a) a sketch of the setup when the robot is between the manhole and the lateral; (b) estimation results for setup (a). The blue stars in (b) indicate the true lengths of the four pipe sections shown in (a).

The work also makes use of the modal decomposition to include in the analysis the plane wave and the first non-axisymmetric mode to extend the usable frequency range. The axial alignment of the linear microphone array facilitates the accurate determination of an artefact's direction relative to the robot's position, marking it very useful for condition localization, classification and for robot navigation. It also enables us to compensate for unwanted reverberation effects from a manhole.

The proposed technique has been tested successfully against experimental data obtained in a realistic drainage pipe with a blockage, manhole, lateral connection and rigid termination. The results demonstrate the capability to determine the direction to an artefact and its location with an accuracy of better than 3 % with respect to the true distance. This accuracy has been achieved through the analysis of the
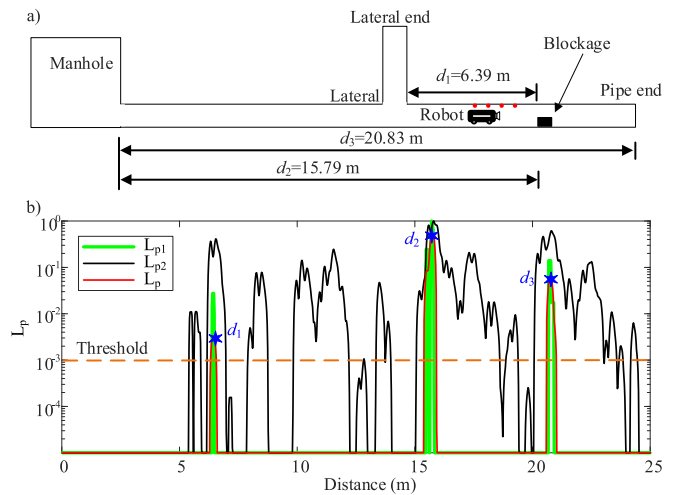

Fig. 12. The estimations of the pipe section lengths: (a) a sketch of the setup when the robot is between the lateral and the blockage; (b) estimation results for setup (a). The blue stars in (b) indicate the true lengths of the four pipe sections shown in (a).

acoustic signals corresponding to the plane wave ($f < f_{10}$) and first non-axisymmetric mode ($f < f_{02}$) frequency regimes. It has been also possible to use the acoustic signatures recorded with this technique to distinguish between blockages and lateral connections because of significant differences in the cross-section pattern in the acoustic pressure waves reflected from these artefacts and their spectral composition. Additionally, the paper has introduced the formulation of a robust algorithm that accurately estimates the length of the pipe sections within 2 % of the actual length.

The proposed technique offers a potential for significantly enhancing diagnostic precision in the assessment of pipeline integrity and configuration with audible acoustic waves and relatively inexpensive acoustic and data acquisition equipment. The work lays a foundational framework for advanced acoustic methodologies to inspect buried pipes with autonomous mobile robots, heralding a new era in the maintenance and monitoring of underground infrastructure. This work also suggests that that uncertainties caused by the presence of sensing platform need a

further investigation to minimise its effect on the recorded acoustic signal.

CRediT authorship contribution statement

Yicheng Yu: Writing – review & editing, Writing – original draft, Visualization, Validation, Software, Methodology, Investigation, Formal analysis, Data curation, Conceptualization. **Pengcheng Shi:** Writing – review & editing, Writing – original draft, Visualization, Validation, Investigation, Funding acquisition, Data curation. **Anton Krynkin:** Writing – review & editing, Writing – original draft, Visualization, Supervision, Resources, Methodology, Funding acquisition, Conceptualization. **Kirill V. Horoshenkov:** Writing – review & editing, Writing – original draft, Visualization, Supervision, Resources, Project administration, Methodology, Funding acquisition, Conceptualization.

Declaration of competing interest

The authors declare the following financial interests/personal relationships which may be considered as potential competing interests: Kirill V Horoshenkov reports financial support was provided by Engineering and Physical Sciences Research Council.

Data availability

Data will be made available on request.

Appendix A

Table A1

Algorithm 1 – Frequency domain Sparse Representation estimation with ℓ_1-norm regularization with SpaRSA [20] to localize artefacts in a pipe.

Task: To estimate the location of artefacts in the pipe $\widehat{\mathbf{s}}$

Input: Excitation chirp signal $A_{00}(t)$, response signal from 4 microphones $\mathbf{P}_j(t) j = 0:3$

Plane wave reconstruction: $\mathbf{P}(t) = \sum_{j=0}^{3} \mathbf{P}_j(t)$

Fast Fourier transform (FFT): $\mathbf{p}(\omega) = \mathscr{F}\{\mathbf{P}(t)\}$, $A_{00}(\omega) = \mathscr{F}\{A_{00}(t)\}$.

Transfer matrix: $\mathbf{H}(\omega, \mathbf{z}_q)$, given by Eqs. (6)(9) for plane wave regime, Eqs. (8)(9) for first non-axisymmetric mode regime

Initialization: $k = 1$, $\mathbf{A} = \mathbf{H}$, $\mathbf{x}_1 = \mathbf{p}$, $\tau_1 \mathbf{I} = \mathbf{A}^T \mathbf{A}$, tolerance $\varepsilon = 10^{-5}$ [20], parameter $\lambda = 0.001$ [20]

Iteration:

   1. $\lambda_k = \max\{0.1\|\mathbf{A}^T \mathbf{x}_k\|_{\infty}, \lambda\}$ [20].

   2. Use [20]: $\mathbf{s}_{k+1} = \text{shrink}(\mathbf{s}_k - \mathbf{A}^T(\mathbf{A}\mathbf{s}_k - \mathbf{x})/\tau_k, \lambda_k/\tau_k)$ referred to as soft shrinkage, where $\text{shrink}(s_i, \lambda) = \text{sgn}(s_i)\max\{|s_i| - \lambda, 0\}$

   3. Update the step size [20]: $\tau_k = \dfrac{(\mathbf{s}_{k+1} - \mathbf{s}_k)^T(\nabla\vartheta(\mathbf{s}_{k+1}) - \nabla\vartheta(\mathbf{s}_k))}{(\mathbf{s}_{k+1} - \mathbf{s}_k)^T(\mathbf{s}_{k+1} - \mathbf{s}_k)}$, where $\nabla\vartheta(\mathbf{s}_k) = \mathbf{A}^T(\mathbf{A}\mathbf{s}_k - \mathbf{x})$

   4. If $\dfrac{\|\mathbf{s}_{k+1} - \mathbf{s}_k\|}{\mathbf{s}_k} \leq \varepsilon$, go to step 5. Otherwise, return to step 2 [20]

   5. $\mathbf{x}_{k+1} = \mathbf{x}_k - \mathbf{A}\mathbf{s}_{k+1}$

   6. If $\lambda_k \leq \lambda$, stop; Otherwise $k = k + 1$, and return to step 1.

Output: $\widehat{\mathbf{s}} = \mathbf{s}_k$.

References

[1] GOV.UK, "Water and treated water" [Online]. Available: https://www.gov.uk/government/publications/water-and-treated-water/water-and-treated-water. [Accessed 01 07 2024].

[2] T.L. Nguyen, A. Blight, A. Pickering, G. Jackson-Mills, A.R. Barber, J.H. Boyle, R. Richardson, M. Dogar, N. Cohen, Autonomous control for miniaturized mobile robots in unknown pipe networks, Front. Robot. AI 9 (2022) 997415.

[3] Y. Yu, A. Safari, X. Niu, B. Drinkwater, K.V. Horoshenkov, Acoustic and ultrasonic techniques for defect detection and condition monitoring in water and sewerage pipes: A review, Appl. Acoust. 183 (2021) 108282.

[4] Y. Yu, A. Krynkin, K.V. Horoshenkov, Modal coupling analysis of the acoustic wave scattering from blockage in a pipe, J. Sound Vib. 588 (2024) 118522.

[5] J.M. Aitken, M.H. Evans, R. Worley, S. Edwards, R. Zhang, T. Dodd, L. Mihaylova, S.R. Anderson, Simultaneous localization and mapping for inspection robots in water and sewer pipe networks: A review, IEEE Access 9 (2021) 140173–140198.

[6] Y. Yu, R. Worley, S. Anderson, K.V. Horoshenkov, Microphone array analysis for simultaneous condition detection, localization, and classification in a pipe, J. Acoust. Soc. Am. 153 (367) (2023) 367–383.

[7] Y. Yu, K.V. Horoshenkov, S. Tait, Microphone array analysis of the first non-axisymmetric mode for the detection of pipe conditions, J. Acoust. Soc. Am. 155 (1) (2024) 575–587.

[8] J. Benesty, J. Chen, Y. Huang, Microphone array signal processing, Springer Science & Business Media, 2008.

[9] X. Wang, M.S. Ghidaoui, Identification of multiple leaks in pipeline II: Iterative beamforming and leak number estimation, Mech. Syst. Sig. Process. 119 (2019) 346–362.

[10] Z. Hu, S. Tariq, T. Zayed, A comprehensive review of acoustic based leak localization method in pressurized pipelines, Mech. Syst. Sig. Process. 161 (2021) 107994.

[11] R. Worley, Y. Yu and S. Anderson, "Acoustic Echo-Localization for Pipe Inspection Robots," in *2020 IEEE International Conference on Multisensor Fusion and Integration for Intelligent Systems (MFI)*, (2020) p. 160-165.

[12] L. Jing, Z. Li, Y. Li, R.D. Murch, Channel characterization of acoustic waveguides consisting of straight gas and water pipelines, IEEE Access 6 (2018) 6807–6819.

[13] L. Jing, M. Wang, Y. Lu, M. Stojanovic and R. Murch, "Differential orthogonal frequency division multiplexing communication in water pipeline channels," *The Journal of the Acoustical Society of America,* 148 (2020) 2 p. EL130-EL134.

[14] Z. Li, Y. Yu, K.V. Horoshenkov, A comparison of the performance of four acoustic modulation techniques for robot communication in pipes, Int. J. Acoust. Vib. 28 (1) (2023) 98–116.

[15] P.M. Morse, K.U. Ingard, Theoretical acoustics, Princeton University Press, 1986.

[16] Y. Yu, A. Krynkin, K.V. Horoshenkov, The effect of 3D surface roughness on acoustic wave propagation in a cylindrical waveguide, Wave Motion 128 (2024) 103304.

[17] Y. Yu, A. Krynkin, Z. Li, K.V. Horoshenkov, Analytical and empirical models for the acoustic dispersion relations in partially filled water pipes, Appl. Acoust. 179 (2021) 108076.

[18] C.C. Paige, M.A. Saunders, LSQR: An algorithm for sparse linear equations and sparse least squares, ACM Trans. Math. Softw. (TOMS) 8 (1) (1982) 43–71.

[19] S.L. Brunton, J.N. Kutz, Data-driven science and engineering: Machine learning, dynamical systems, and control, Cambridge University Press, 2019.

[20] S.J. Wright, R.D. Nowak, M.A. Figueiredo, Sparse reconstruction by separable approximation, IEEE Trans. Signal Process. 57 (7) (2009) 2479–2493.

[21] K. Buckley, Spatial/spectral filtering with linearly constrained minimum variance beamformers, IEEE Trans. Acoust. Speech Signal Process. 35 (3) (1987) 249–266.

[22] Matlab, "Time delay LCMV beamformer," [Online]. Available: https://ch. mathworks.com/help/phased/ref/phased.timedelaylcmvbeamformer-system-object.html. [Accessed 2024 4 2].

[23] H. L. Van Trees, Optimum array processing., John Wiley & Sons (2002).

[24] O. Frost, An algorithm for linearly constrained adaptive array processing, Proc. IEEE 60 (8) (1972) 926–935.